SLAC-PUB-163
(Revised)
March 1966

ELECTRON INDUCED CASCADE SHOWERS IN COPPER AND LEAD AT 1 GeV*

Walter R. Nelson, Theodore M. Jenkins, Richard C. McCall, Joseph K. Cobb
Stanford Linear Accelerator Center
Stanford University, Stanford, California

Abstract

The radial and longitudinal development of electron-photon showers has been measured in copper and lead at 1 Gev. A new technique[20] using the thermoluminescent property of LiF has been employed to measure energy deposition. The resultant radial distributions and transition curves show good agreement with Monte Carlo calculations.

(Submitted to Physical Review)

*Work done under the auspices of the U. S. Atomic Energy Commission.

I. INTRODUCTION

When a high energy electron or photon enters an absorber, an electromagnetic cascade shower is produced. The basic interactions of the electrons and photons are well established, but the analytical solutions of the diffusion equations which describe the shower are prohibitively difficult to obtain. Rossi and Greisen[1] concentrated on the longitudinal shower development using various approximations. The lateral and angular spread was derived by Kamata and Nishimura[2] but has application only to high energy cosmic ray phenomena. Another analytical set of solutions has been presented for the longitudinal development by Belenkii and Ivanenko.[3] The most useful calculations are the Monte Carlo studies, which take into account the important cross-section data, and which do not introduce as many oversimplifications. These were first done by Wilson[4] and then more elaborately by Messel, et al.,[5] and Zerby and Moran.[6] Most recently Nagel[7] and Völkel[8] have improved the shower calculations in lead by lowering the cut-off energy.

Experimental measurements of shower propagation have been made using ionization chambers,[9] scintillators,[10] photographic film,[11] spark chambers,[12, 13] cloud chambers,[14] nuclear emulsions,[15] Cerenkov counters,[16] and bubble chambers.[17] All of these methods have some disadvantages, especially for measuring radial development of the showers. Some of these disadvantages are limited intensity range of the detector, large energy dependence, large physical size, laborious methods, and disturbance of the shower by the detector. In addition, those methods which make measurements point by point require long machine time and careful monitoring and data normalization to correct for variations in beam intensity.

The recent development of thermoluminescent dosimetry (TLD)[18] seemed to offer an excellent tool for the investigation of shower development, and a preliminary experiment using LiF (TLD-700 Harshaw Chemical Co.)[19] has been published.[20] This detector was chosen because it has a flat energy response (Fig. 1), is linear over a wide dose range (Fig. 2), and has good precision over this range (Fig. 3).

Essentially the introduction of a small volume of LiF into an absorber satisfies the requirements of a Bragg-Gray cavity[21] and hence is a measure of the energy loss in the surrounding medium. An advantage of using TLD to measure energy deposition is that beam intensity monitoring is unnecessary, other than requiring the absorbed dose in the LiF to be less than saturation ($\sim 10^5$ R) at shower maximum. This is true because the LiF detectors are integrating devices, have high sensitivity and hence respond to small doses, and all of the detectors can be exposed in the absorber simultaneously.

This experiment uses the TLD method to measure the three-dimensional cascade in lead and copper at 1 GeV using the Stanford Mark III electron accelerator. The results should be useful in determining the efficiency of a total absorption type detector.

II. EXPERIMENTAL PROCEDURE

Powdered TLD-700 LiF was funneled into thin-walled teflon tubing (0.048-inch o.d., 0.034-inch i.d.) using a vibrator tool to obtain uniform packing, and the tubes were plugged at both ends. The bulk density was measured to be 1.64 g/cm^{-3}. The copper consisted of plates which were stacked to form a 12" × 12" × 24" absorber (Fig. 4). The middle plate was

grooved to hold the tubes. The lead absorber was in the form of 6" × 6" x 1/4" plates, separated by air gaps of 0.050 inch, in which the LiF-loaded tubing was positioned (Fig. 5).

Using a glass plate, the beam spot size was found to be almost circular with a diameter of less than 1/16 inch. The beam energy was 1000 ± 10 MeV. Beam alignment is more critical in this experiment than in similar experiments where the beam position may be found by trial and error during the course of the experiment. For accurate positioning, two ZnS screens were placed at the front and rear of the absorber, and with the absorber removed, the beam line determined. Using a transit, the LiF-loaded absorber was then positioned such that the beam struck the middle of the first and last detectors located in the absorber.

After the exposures were made the detectors were removed from the blocks and subsequently analyzed over a period of one month. There is less than 5% per year decay of the thermoluminescence at room temperature.[22] Each teflon tube was cut into segments, the LiF vibrated out and weighed, and the light output measured with a commercially available TLD reader (Controls for Radiation, Inc.). The smallest segment that was capable of being handled was 0.185 cm in length, which yielded about 0.9 mg of phosphor. This placed a limit on the resolution of the detector. The smallest segments were taken around the peak of the profile, but larger segments were required on the sides because the energy deposition was considerably less and good resolution was not necessary there. Radial resolution is poorest at the front of the absorber where the shower has not spread very much, and becomes progressively better further into the block.

LiF powder from each cut was weighed on a torsion balance (Vereenigde Draadfabricken, Holland) which can weigh to ± 0.025 mg, i.e., to about ± 3% for the smallest samples. Figure 2 was then used to determine the absorbed energy,

and a profile curve obtained from all the readings in a string. Zero radius was independently determined for each string by plotting the segment readings, and finding the line about which the resultant curve was symmetrical.

III. EXPERIMENTAL RESULTS

Table I (A through N) lists the data from the radial energy deposition measurements in LiF at various depths in lead. Table II (A through K) lists the same thing for copper. The energy deposition has been normalized to sample weight. In Figs. 6 and 7 the normalized energy deposition versus the radial distance is plotted for lead and copper, respectively. The center of each of these profile curves was chosen by symmetry. Data points for representative depths are included on each figure. The measurement errors are only slightly larger than the data circles themselves.

IV. COMPARISON OF EXPERIMENT WITH MONTE CARLO CALCULATION

A comparison between calculation and experiment requires that a consistent choice of radiation length and critical energy values be used. Dovzhenko and Pomanskii[23] have pointed out that in the calculation of the radiation length units, various authors took different account of the influence of the total screening, of the processes in the field of the atomic electrons, and of the inaccuracy of the Born approximation. This has caused the values of the radiation length units to differ by 10-20%, which in turn has led to a discrepancy in the values of the critical energies. They analyzed the causes of these discrepancies and listed values for radiation lengths and critical energies of common substances, along with equations to determine such values for complex substances. We have used their values (Table III) throughout this paper (except in Fig. 8).

A comparison of three Monte Carlo calculations for a 1 GeV electron-initiated shower in lead with a 10 MeV cut-off is shown in Fig. 8, where there is excellent agreement. The choice of the cut-off energy significantly affects the shape of the transition curve.[6,7,8] Both for particle density and energy deposition, lowering the cut-off energy shifts the peak deeper into the shower and decreases (flattens) the slope in the tail. For comparison purposes we would like a calculation which uses a cut-off energy corresponding to that of LiF ($\sim$ 2 eV). The calculation for lead with the lowest cut-off energy is by Nagel[7] (E_e = 1.5 MeV, E_γ = 0.25 MeV), and for copper is by Zerby and Moran[6] ($E_e = E_\gamma$ = 2 MeV).

The amount of energy that is deposited in a cylindrical ring of volume $2\pi r\, dr\, dt$ at a distance r from the shower axis and at a depth t in the shower is given by E(r,t). Figure 9a shows a comparison of the Monte Carlo copper calculation with the present experiment and they appear to agree quite well. A similar comparison is made for lead in Fig. 9b where the agreement is not as good. Since the lead absorber consisted of alternate layers of lead and air, a correction was made to account for the purely geometric spread. We chose to view the absorber as a homogeneous mixture of lead and air with an apparent density of 9.5 g/cm^3. This is probably a good approximation deep in the shower; however, it is not accurate in the first few strings.

Since the Monte Carlo calculation is based on a delta function type incident electron, while our beam was of a finite size, we would expect that the measured E(r,t) histogram could be wider than the calculated one for a given depth. At greater depths the effect of a finite beam size should decrease. At the depths chosen in Fig. 9a for copper, the effect of the beam size is not noticible. The experimental histogram at 10 radiation lengths for lead in Fig. 9b is closer to the Monte Carlo histogram than that at 2.25 radiation lengths.

Energy transition curves (longitudinal positron versus fraction of energy deposited per radiation length) can be obtained from

$$\frac{\Delta E(t)}{E_o} = \frac{\int_0^\infty E(r,t)\,dr}{\int_0^\infty \int_0^\infty E(r,t)\,dr\,dt}$$

The integrations were performed graphically and the resultant transition curves for the copper and lead experiments were compared with Monte Carlo calculations (Figs. 10 and 11).

The slopes in the case of copper (Fig. 10) agree, but the measured position of the shower maximum is deeper by approximately 0.75 radiation length than that calculated by Zerby and Moran[6] using a cut-off energy of 2 MeV. One would expect even closer agreement if the cut-off energy were lowered. This is because the tail of the shower is predominantly due to photons which most probably have energies close to the minimum of the mass absorption curve. The Pb curve calculation which carries photons to 0.25 MeV will not be significantly affected since the range of 0.25 MeV photons is short in Pb. In the case of copper, the cut-off energy is 2 MeV where the photon range is considerable. Inclusion of lower energy photons will tend to carry the energy of the shower deeper. This is clearly shown in the calculations of Zerby and Moran.[6]

It has been suggested by Pinkau[24] that a large change in the critical energy prior to the depth at which the cascade is measured could result in some distortion of the shower. For both the Pb and the Cu, the effect of the LiF is too small to detect due to the small tubing diameter.

It would be interesting to compare the slope of the measured transition curve with a simple model; namely, the shower propagation after the maximum is due to photons having the lowest absorption coefficient. This has been done

by Nagel,[7] Völkel,[8] and Lengeler,[17] who concluded that the model was too simple. They compared $e^{-\lambda_{min} t}$ with transition curves for particle number using the minimum attenuation coefficient. Since we are measuring energy deposition, it seems more reasonable to use the energy absorption coefficient. Both slopes corresponding to attenuation and absorption are shown in Figs. 10 and 11. The absorption slope, in the case of copper, is close to both the measured and Monte Carlo slopes. The agreement is not as good in the case of lead. The model is probably too simple.

To determine the efficiency of a total absorption type detector, a knowledge of the fraction of the energy that escapes,

$$\frac{U(r)}{E_o} = \frac{\int_0^\infty \int_r^\infty E(r,t)\, dr\, dt}{\int_0^\infty \int_0^\infty E(r,t)\, dr\, dt} ,$$

for various cylindrical volumes is useful. Figure 12 gives U/E_o versus radius in Molière units for lead and copper. A Molière unit, r_1, is the characteristic measure for radial distributions in analytic shower theory,[25] and is equal to $X_o E_s / \epsilon_o$, where ϵ_o is the critical energy of the material, X_o is the radiation length, and $E_s = 21.2$ MeV. Again there is good agreement between this experiment and Monte Carlo calculation. The Monte Carlo calculations are for cylinders of infinite length, whereas the experimental absorbers were fairly long, but finite.

By plotting the radial size in Molière units, the copper and lead curves nearly coincide. It would be convenient if all of the curves coincided not only independently of choice of absorber, but also of incident energy. Figure 13 shows that this is the case for Monte Carlo calculations. It is interesting to see how other experiments agree with Monte Carlo calculations when plotted in this manner. Figure 14 shows that Murata[11] is not too far from agreeing with the Monte Carlo calculation whereas the Kantz and Hofstadter[10] results do not agree.

V. SUMMARY

The use of thermoluminescent dosimetry techniques to measure longitudinal and radial shower propagation has proved to be quite effective. At 1 GeV incident electron energy, the radial energy deposition curves have been measured and found to agree quite well with Monte Carlo predictions. The energy transition curves in lead and copper, obtained by integrating the radial distributions, agree very well in the case of copper, and reasonably well for lead.

The fraction of incident energy that escapes an infinitely long cylinder of radius r in Molière units is plotted and it is observed that most of the existing Monte Carlo and experimental data, including this experiment, coincide independently of choice of absorber and incident energy.

Acknowledgement

The authors wish to express their appreciation to Professor Robert Mozley for allowing us to use his time on the Stanford Mark III accelerator, and for his assistance in making the exposures. We also wish to thank Mr. Edward Wilson for reading the data after the exposures, and Mr. Thomas Ginn for helping him in reducing the data to its present form.

FOOTNOTES AND REFERENCES

1. B. Rossi and K. Greisen, Rev. Mod. Phys. 13, 240 (1941).
2. K. Kamata and J. Nishimura, Prog. Theor. Phys. (Kyoto) 6, 93 (1958).
3. S. Z. Belenkii and I. P. Ivanenko, Soviet Phys.--Usp. 2, 912 (1960).
4. R. R. Wilson, Phys. Rev. 86, 261 (1952); Wilson's original results have been corrected by H. Thom, Phys. Rev. 136, B447 (1964).
5. H. Messel, A. D. Smirnov, A. A. Varfolomev, D. F. Crawford, and J. C. Butcher, Nucl. Phys. 39, 1 (1962).
   D. F. Crawford and H. Messel, Nucl. Phys. 61, 145 (1965).
   D. F. Crawford and H. Messel, Phys. Rev. 128, 2352 (1962).
6. C. D. Zerby and H. S. Moran, Oak Ridge National Laboratory Reports Nos. ORNL-3329 (1962) and ORNL-TM-422 (1962); J. App. Phys. 34, 2445 (1963). Also, a calculation for 950 MeV electrons incident on copper, with a cut-off energy of 2 MeV, was done for the Stanford Linear Accelerator Center (private communication).
7. H. H. Nagel, Zeit. für Phys. 186, 319 (1965).
8. U. Völkel, Deutsches Elektronen-Synchrotron Report No. DESY 65/6 (July 1965).
9. W. Blocker, R. W. Kenney, and W. K. H. Panofsky, Phys. Rev. 79, 419 (1950).
10. A. Kantz and R. Hofstadter, Phys. Rev. 89, 607 (1953); Nucleonics 12, 36 (1954).
11. Y. Murata, J. Phys. Soc. Japan 20, 209 (1965).
12. J. W. Cronin, E. Engles, M. Pyka, and R. Roth, Rev. Sci. Instr. 33, 946 (1962).
13. R. Kajikawa, J. Phys. Soc. Japan 18, 1365 (1963).

14. M. D. Wilson and I. B. McDiarmid, Can. J. Phys. 40, 573 (1962).

15. M. Akashi, K. Shimizu, Z. Watanabe, T. Ogawa, N. Ogita, A. Misaki, I. Mito, S. Oyama, S. Tokunaga, M. Fujimoto, S. Hasegawa, J. Nishimura, K. Niu, and K. Yokoi, J. Phys. Soc. Japan 17, Suppl. A-III, Part III, 427 (1962).

16. C. A. Heusch and C. Y. Prescott, Phys. Rev. 135, B772(1964).

17. H. Lengeler, W. Tejessy, and M. Deutschmann, Zeit. für Phys. 175, 283 (1963).

18. F. H. Attix, Naval Research Laboratory Report No. NRL-6145 (1964).

19. A solid-state material which absorbs the energy of ionizing radiation in deep traps, giving off light when subsequently heated.

20. T. M. Jenkins, J. K. Cobb, W. R. Nelson, and R. C. McCall, Nucl. Instr. and Methods 37 (1), 174 (1965).

21. F. W. Spiers, Radiation Dosimetry (ed. G. J. Hine and G. L. Brownell), (Academic Press, New York, 1956).

22. J. R. Cameron, D. Zimmerman, G. Kenny, R. Buch, R. Bland, and R. Grant, Health Physics 10, 25 (1964).

23. O. I. Dovzhenko and A. A. Pomanskii, Soviet Phys.--JETP 18(1), 187 (1964).

24. K. K. Pinkau, Phys. Rev. 139, B1548 (1965).

25. K. Greisen, Extensive Air Showers, Progress in Cosmic Ray Physics, Vol. III, North-Holland, Amsterdam, 1956.

FIGURE CAPTIONS

1. Energy dependence of LiF. Taken from Cameron, et al.[22]
2. Thermoluminescent response of LiF, measured with Co^{60} gamma rays.
3. Measurement precision using the TLD technique.
4. The copper absorber showing the relative positions of the LiF detectors. (a) Exploded view; (b) Assembled view.
5. A cutaway view of the lead absorber showing the relative positions of the LiF detectors.
6. Energy deposition profile curves for 1 GeV electrons incident on lead. Measured points are shown for a representative depth. Errors are slightly larger than the data circles. Effective density = 9.5 g/cm^3 (see text).
7. Energy deposition profile curves for 1 GeV electrons incident on copper. Measured points are shown for a representative depth. Errors are slightly larger than the data circles.
8. A comparison of three Monte Carlo calculations for an electromagnetic cascade shower initiated by a 1 GeV electron in lead. A cutoff energy of 10 MeV and a radiation length of 5.8 g/cm^{-2} was used.

9a. A histogram plot of E(r,t) for copper, comparing the results of this experiment with a Monte Carlo calculation at two different shower depths.

9b. A histogram plot of E(r,t) for lead, comparing the results of this experiment with a Monte Carlo calculation at two different shower depths.

10. Longitudinal energy deposition in copper. A comparison of this experiment with a Monte Carlo calculation. X_o = 13.0 g/cm^{-2}, ρ = 8.89 g/cm^{-3}.
11. Longitudinal energy deposition in lead. A comparison of this experiment with a Monte Carlo calculation. X_o = 6.4 g/cm^{-2}, ρ = 11.35 g/cm^{-3}.
12. Fraction of the incident energy that escapes various cylindrical volumes. A comparison of this experiment with Monte Carlo calculations.

13. Fraction of the incident energy that escapes various cylindrical volumes. A comparison of Monte Carlo results showing the independence of the choice of absorber and of incident energy.

14. Fraction of the incident energy that escapes various cylindrical volumes. A comparison of Monte Carlo calculations with other experiments.

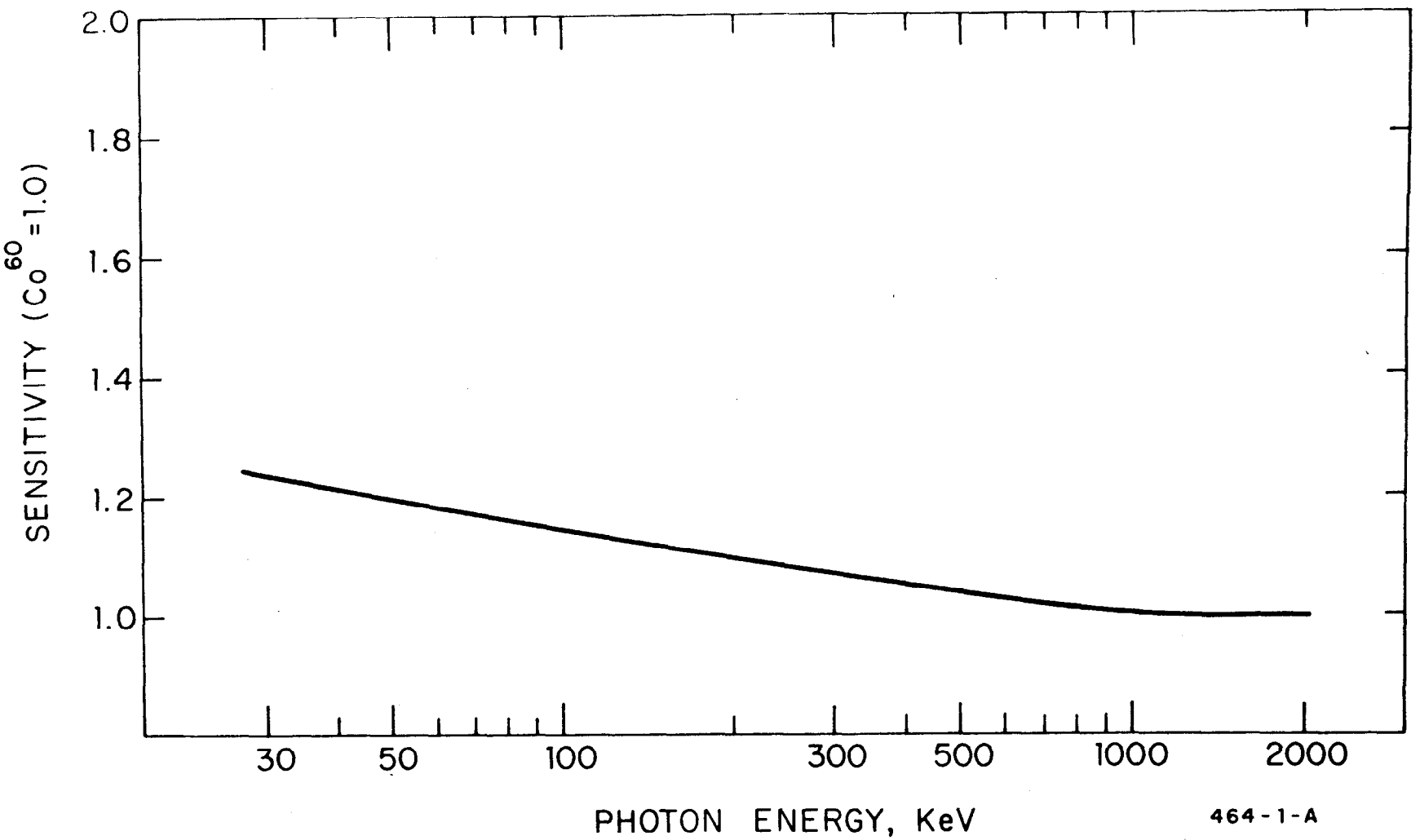
2.0
1.8
1.6
1.4
1.2
1.0
SENSITIVITY (Co^{60}=1.0)
30
50
100
300
500
1000
2000
PHOTON ENERGY, KeV
464-1-A

Fig. 1

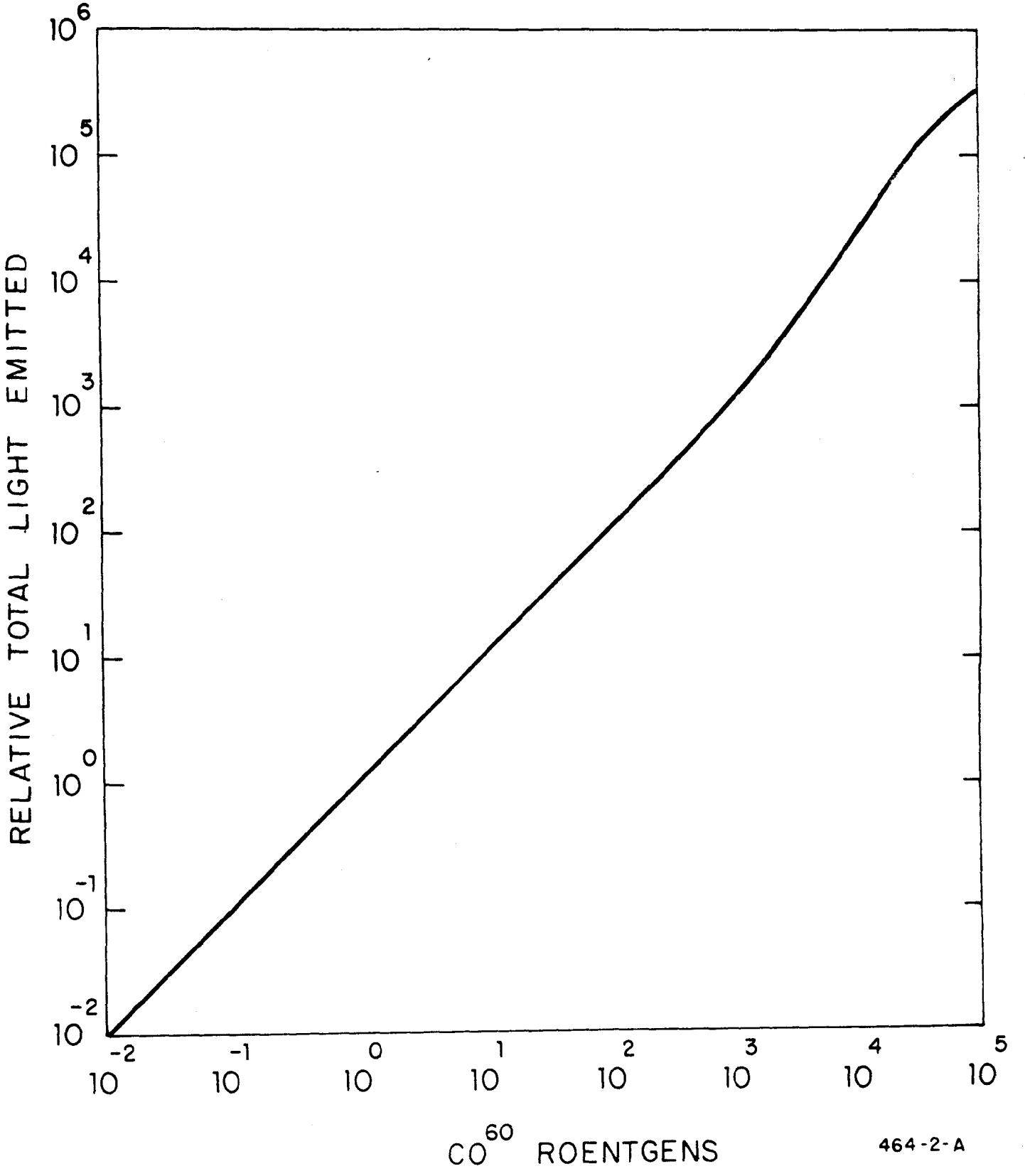
RELATIVE TOTAL LIGHT EMITTED
10^{6}
10^{5}
10^{4}
10^{3}
10^{2}
10^{1}
10^{0}
10^{-1}
10^{-2}
10^{-2} 10^{-1} 10^{0} 10^{1} 10^{2} 10^{3} 10^{4} 10^{5}
CO^{60} ROENTGENS
464-2-A

Fig. 2

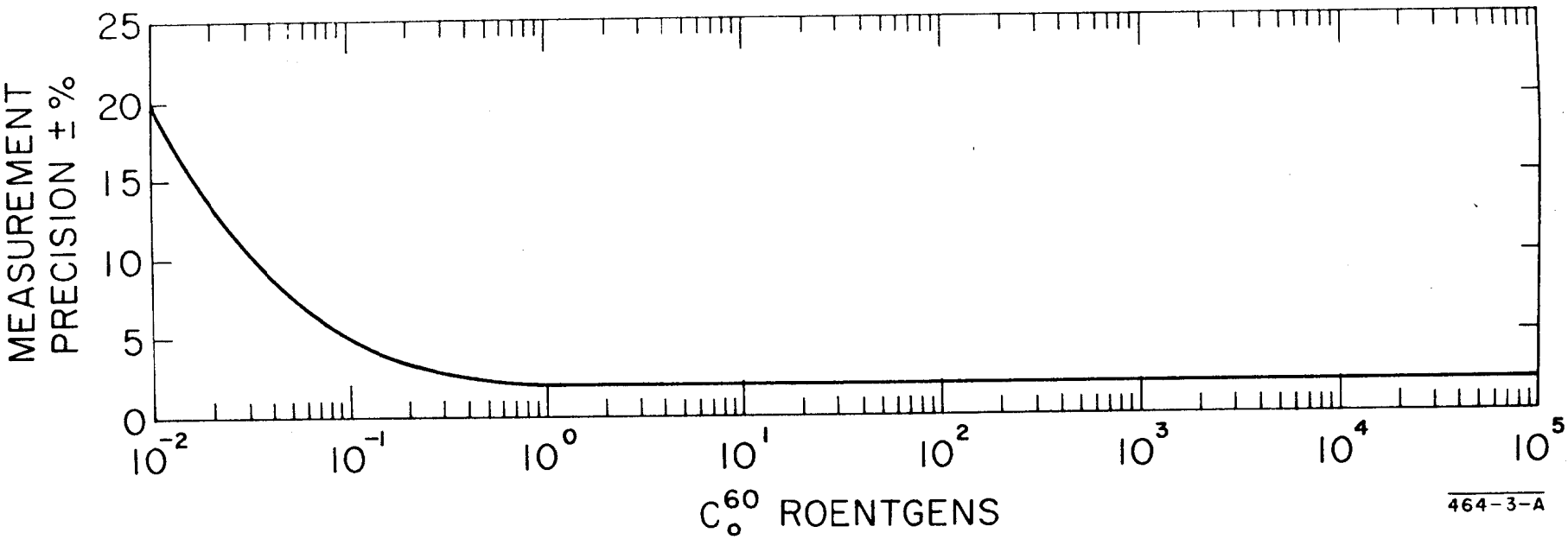
MEASUREMENT
PRECISION ± %
25
20
15
10
5
0
10^{-2}
10^{-1}
10^{0}
10^{1}
10^{2}
10^{3}
10^{4}
10^{5}
C_o^{60} ROENTGENS
464-3-A

Fig. 3

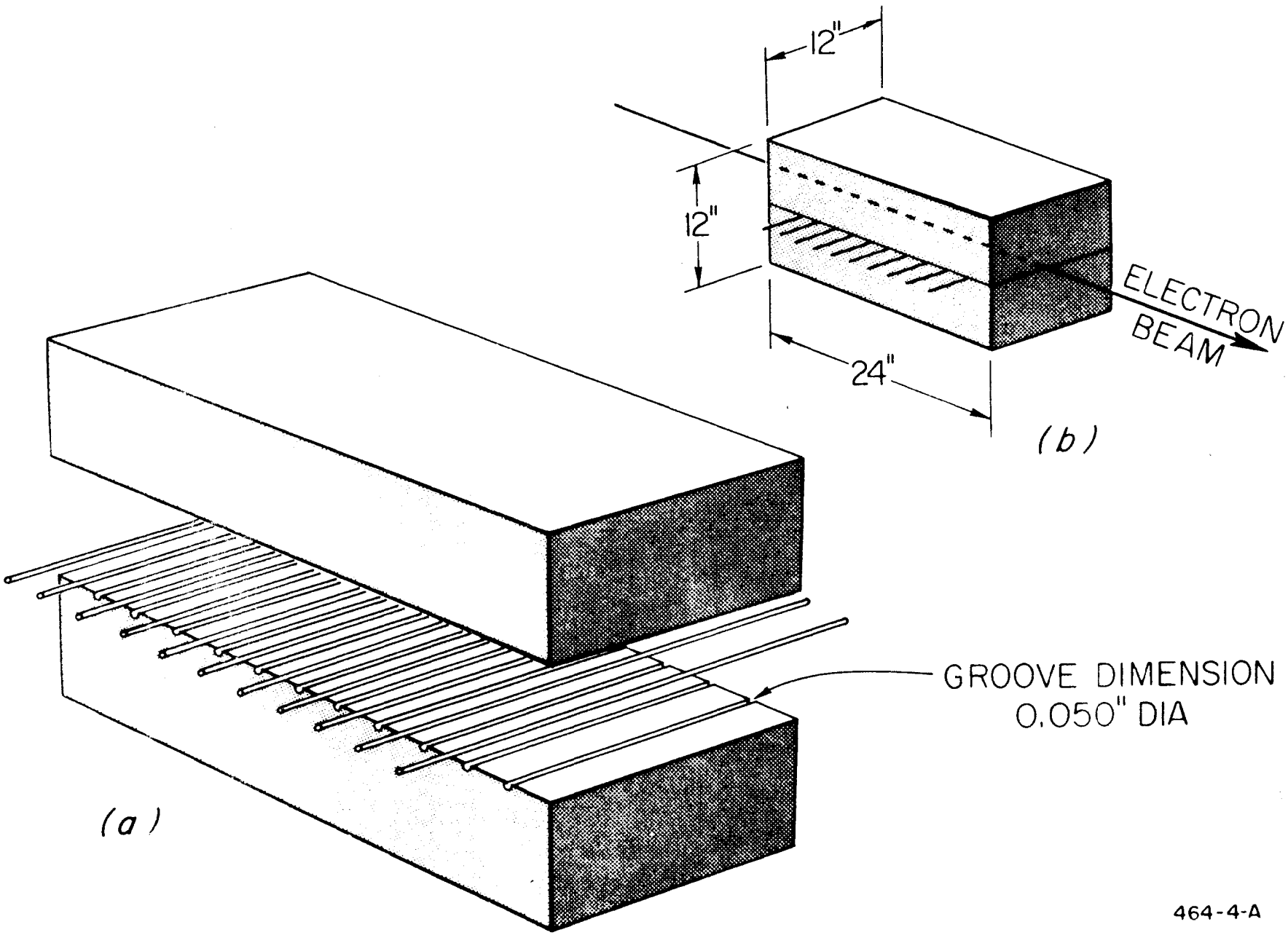

Fig. 4

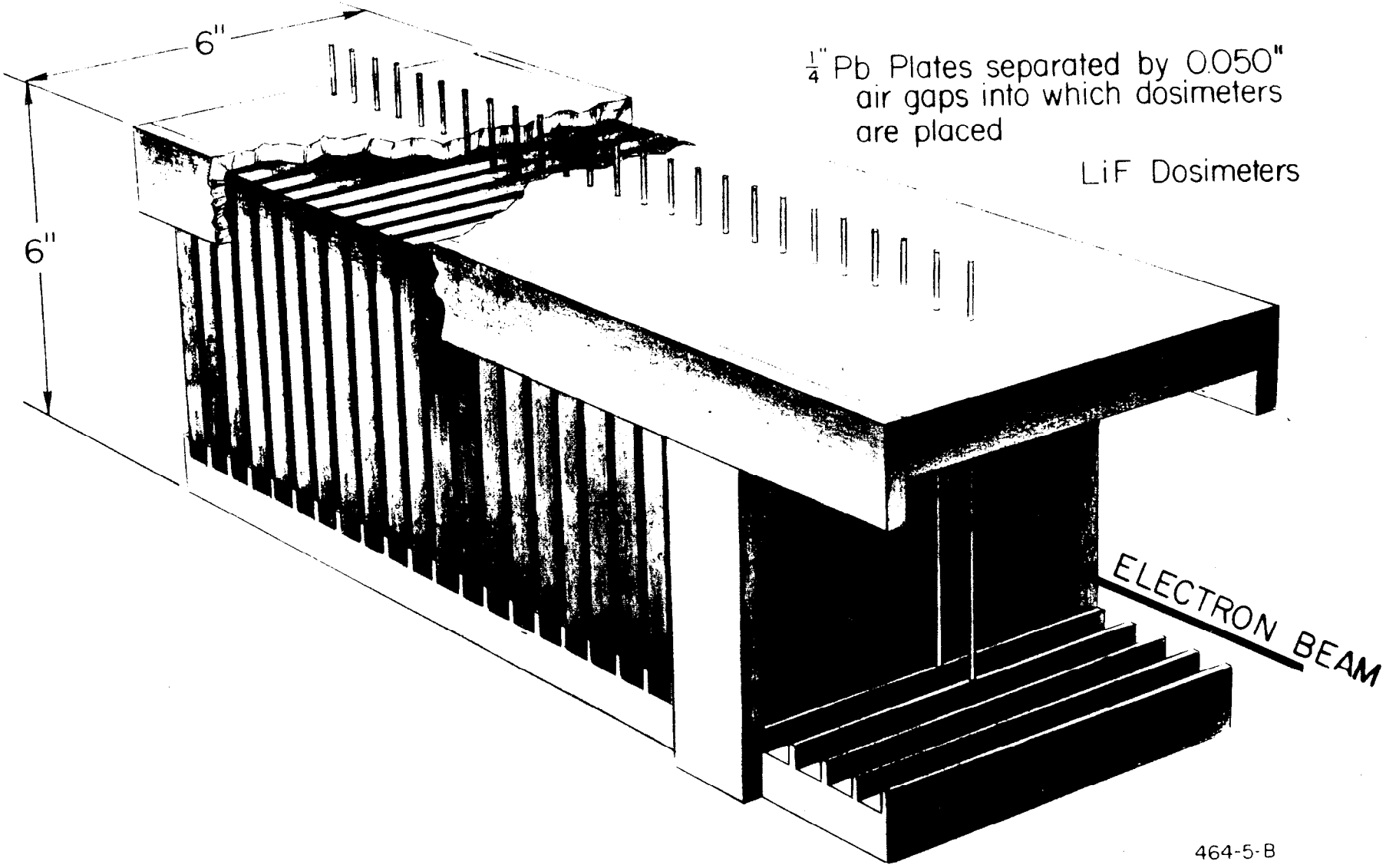

FIG. 5 -- A CUT-A-WAY VIEW OF THE LEAD ABSORBER SHOWING THE RELATIVE POSITIONS OF THE LiF DETECTORS.

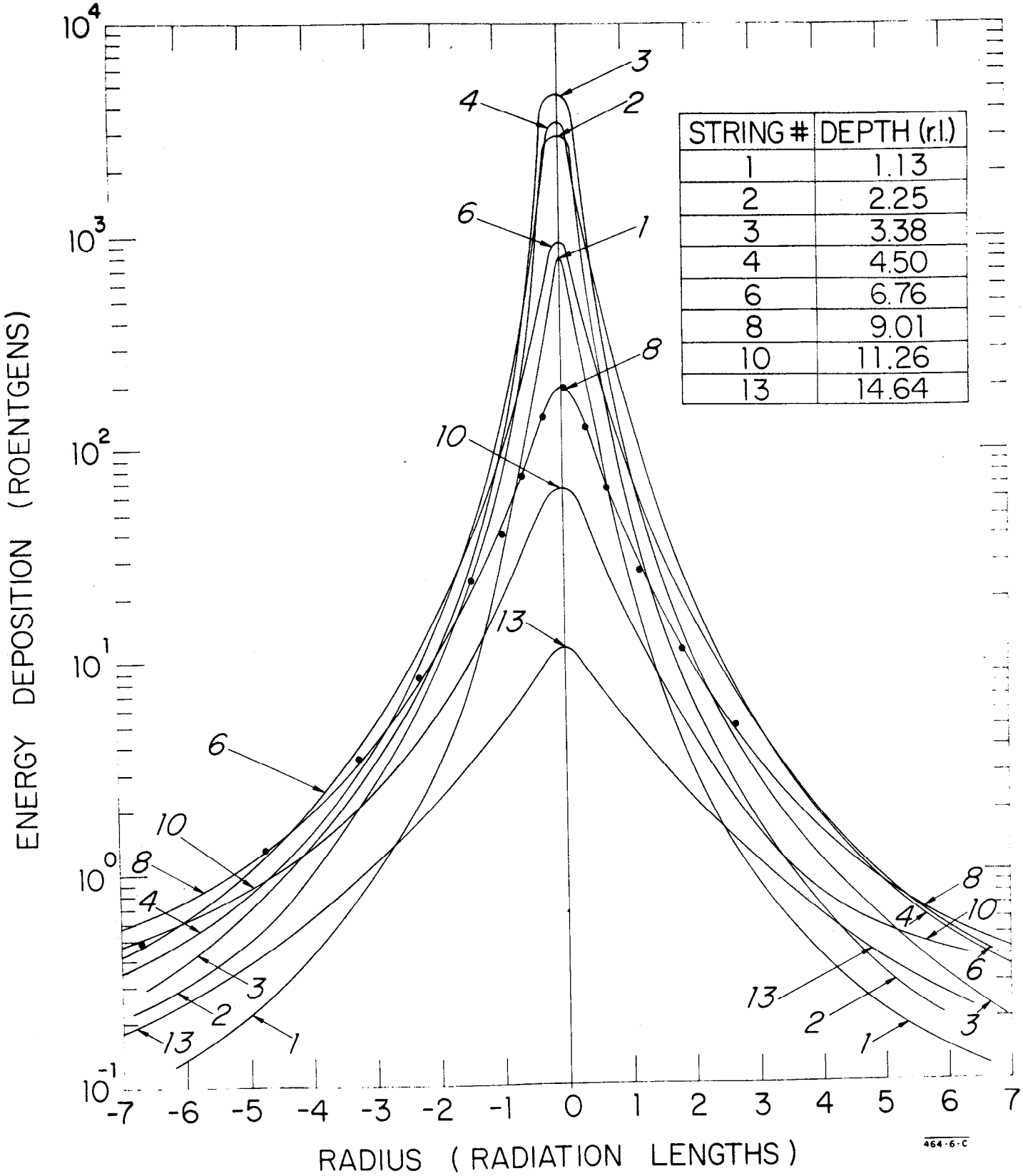
ENERGY DEPOSITION (ROENTGENS)
RADIUS (RADIATION LENGTHS)
STRING # | DEPTH (r.l.)
1 | 1.13
2 | 2.25
3 | 3.38
4 | 4.50
6 | 6.76
8 | 9.01
10 | 11.26
13 | 14.64
464-6-C

Fig.6

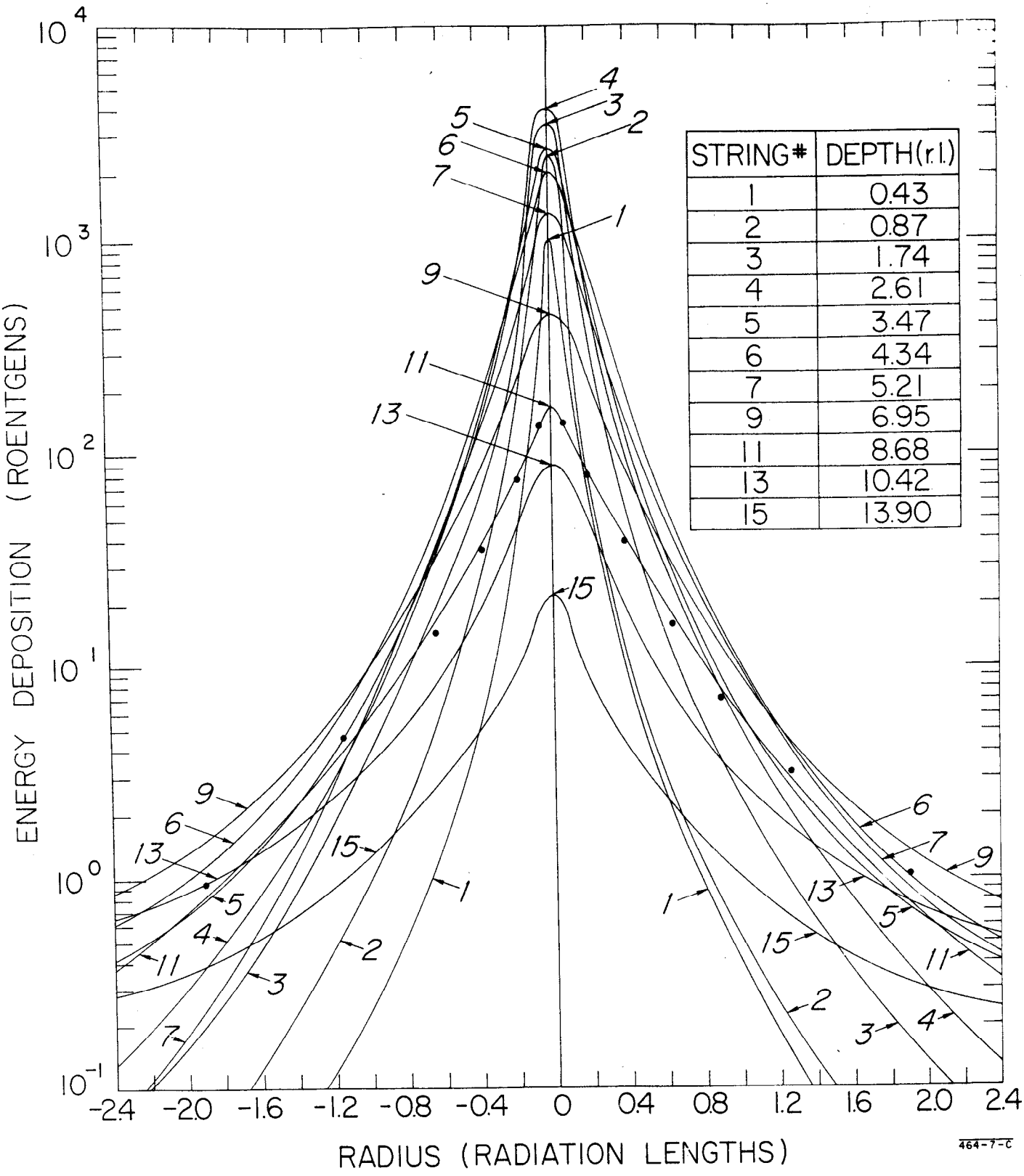
ENERGY DEPOSITION (ROENTGENS)
RADIUS (RADIATION LENGTHS)
STRING# | DEPTH(r.l.)
1 | 0.43
2 | 0.87
3 | 1.74
4 | 2.61
5 | 3.47
6 | 4.34
7 | 5.21
9 | 6.95
11 | 8.68
13 | 10.42
15 | 13.90
464-7-C

Fig. 7

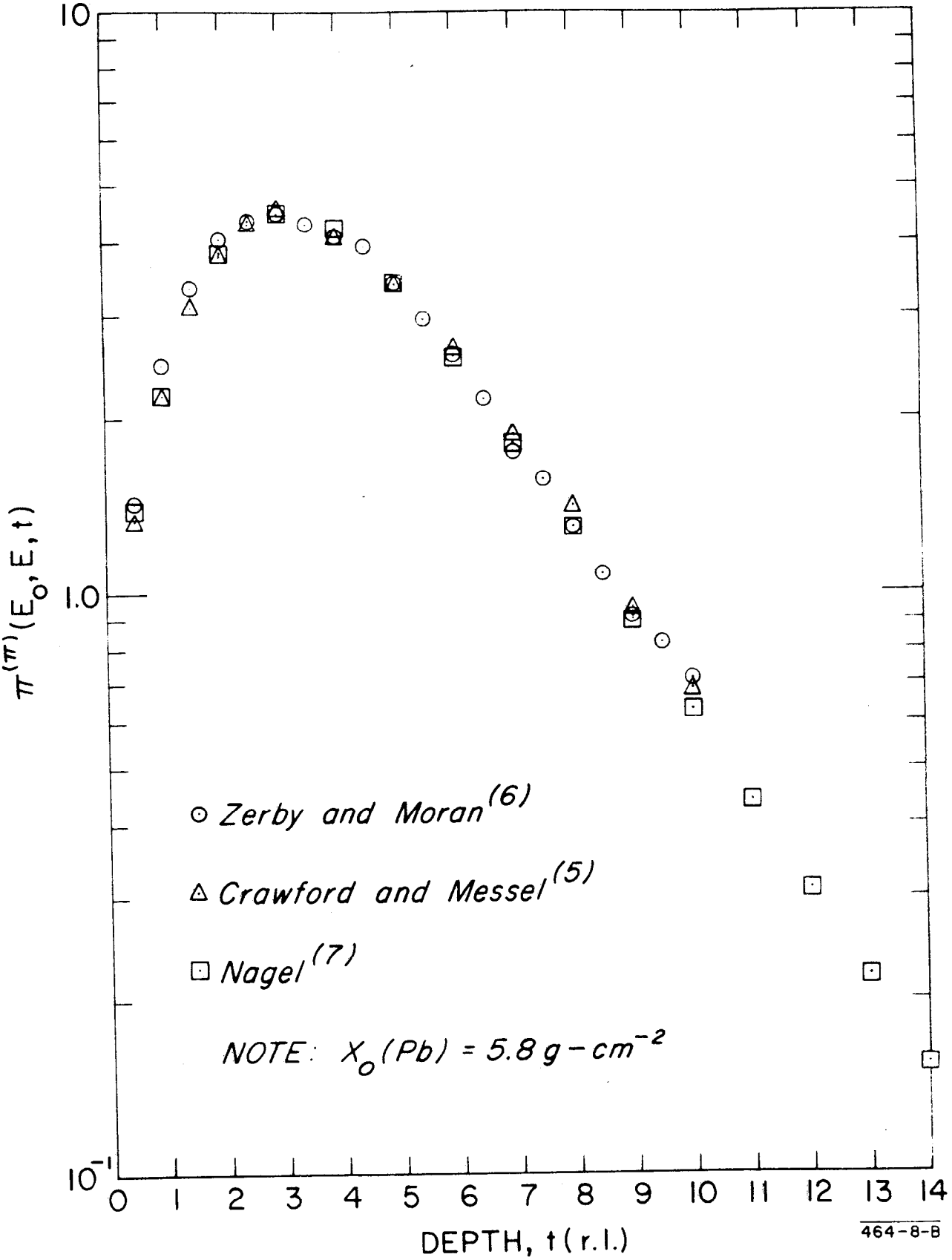
10
1.0
10^{-1}
$\pi^{(\pi)}(E_o, E, t)$
0 1 2 3 4 5 6 7 8 9 10 11 12 13 14
DEPTH, t (r.l.)
Zerby and Moran(6)
Crawford and Messel(5)
Nagel(7)
NOTE: $X_o(Pb) = 5.8\ g-cm^{-2}$
464-8-B

Fig. 8

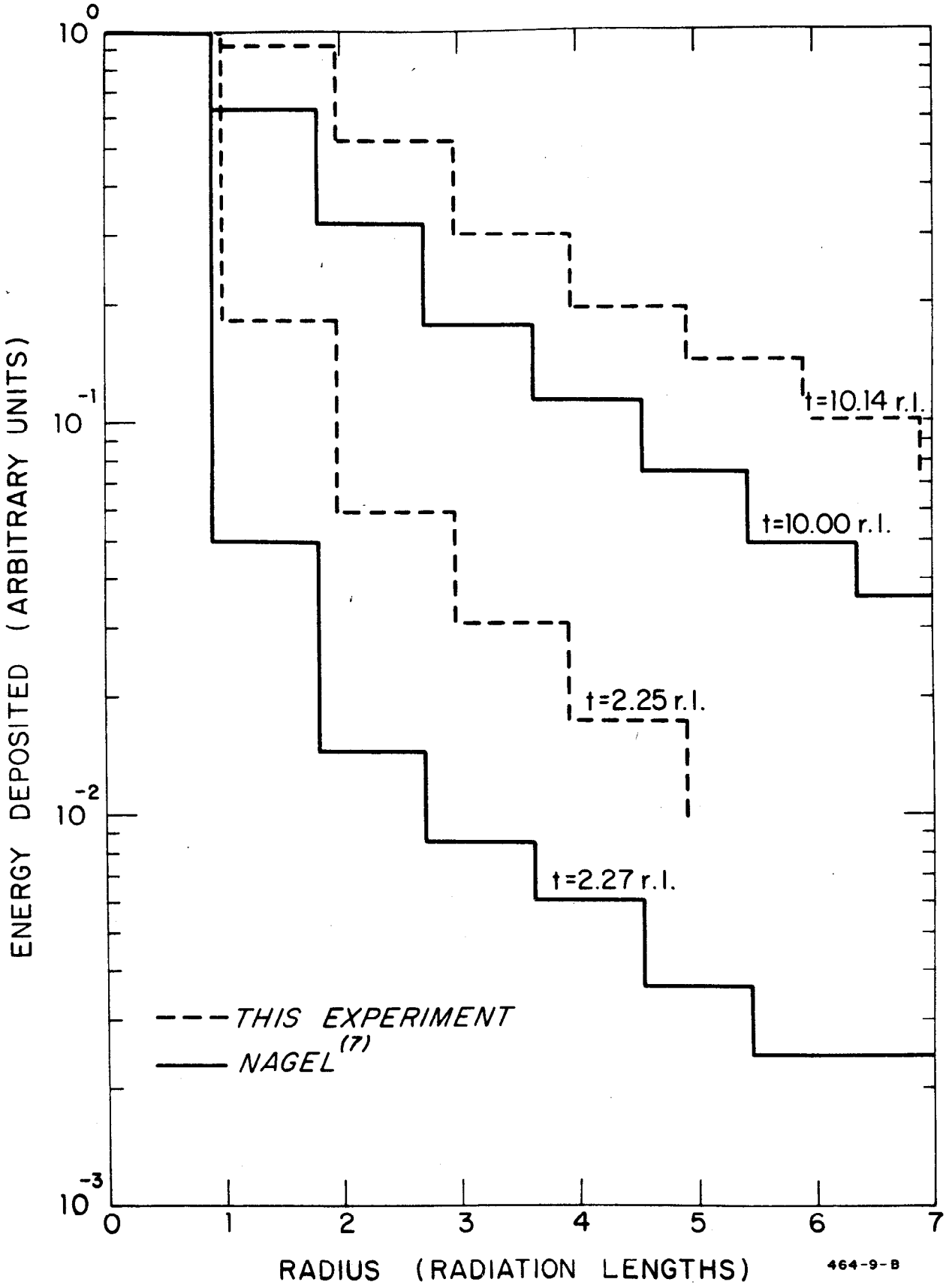
ENERGY DEPOSITED (ARBITRARY UNITS)
10^{0}
10^{-1}
10^{-2}
10^{-3}
t=10.14 r.l.
t=10.00 r.l.
t=2.25 r.l.
t=2.27 r.l.
THIS EXPERIMENT
NAGEL(7)
0
1
2
3
4
5
6
7
RADIUS (RADIATION LENGTHS)
464-9-B

Fig. 9

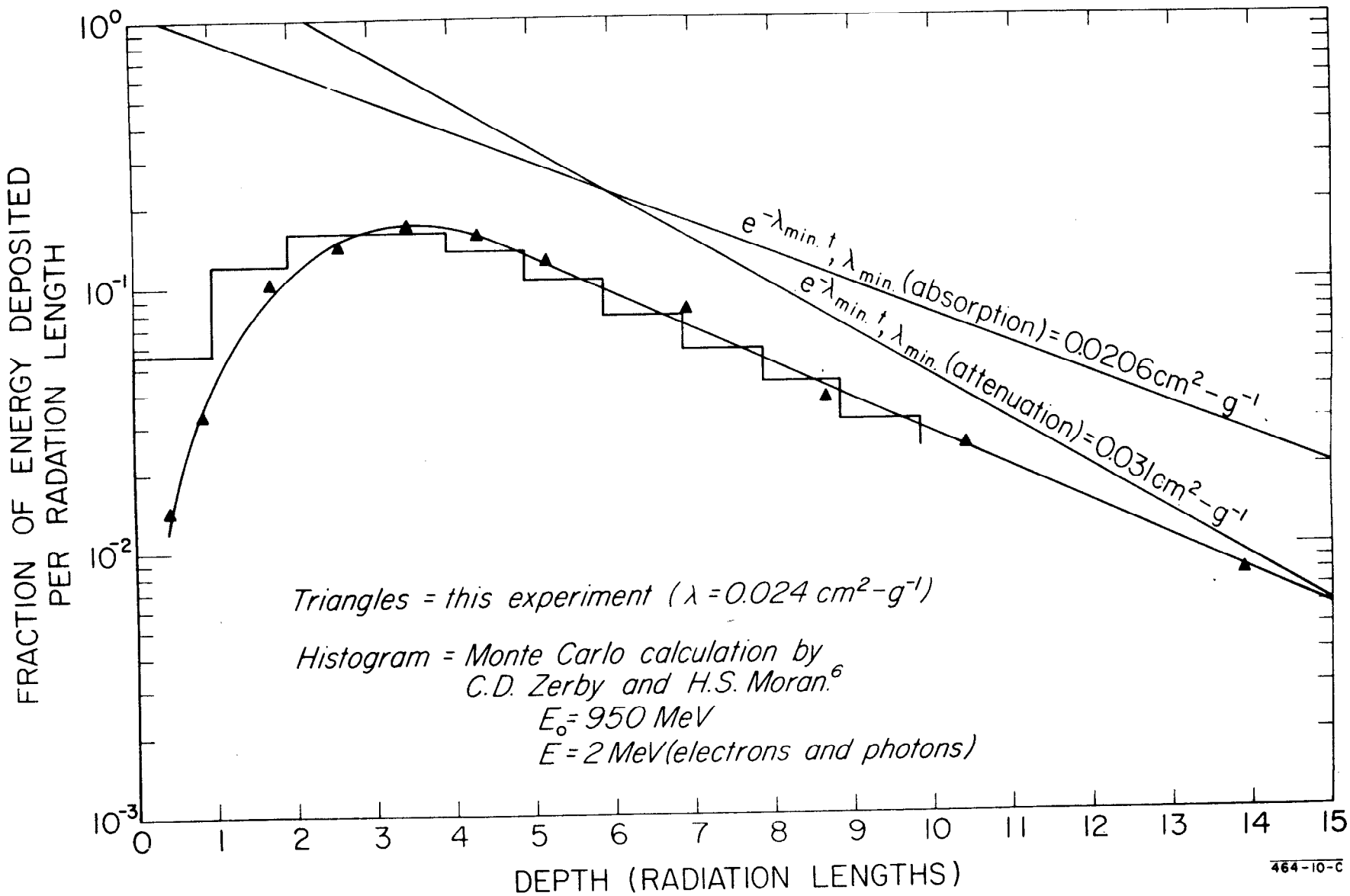
FRACTION OF ENERGY DEPOSITED PER RADIATION LENGTH
10^0
10^{-1}
10^{-2}
10^{-3}
0 1 2 3 4 5 6 7 8 9 10 11 12 13 14 15
DEPTH (RADIATION LENGTHS)
$e^{-\lambda_{min.} t}$, $\lambda_{min.}$ (absorption) = 0.0206 cm^2-g^{-1}
$e^{-\lambda_{min.} t}$, $\lambda_{min.}$ (attenuation) = 0.031 cm^2-g^{-1}
Triangles = this experiment (λ = 0.024 cm^2-g^{-1})
Histogram = Monte Carlo calculation by C.D. Zerby and H.S. Moran.[6]
E_o = 950 MeV
E = 2 MeV (electrons and photons)
464-10-C

Fig. 10

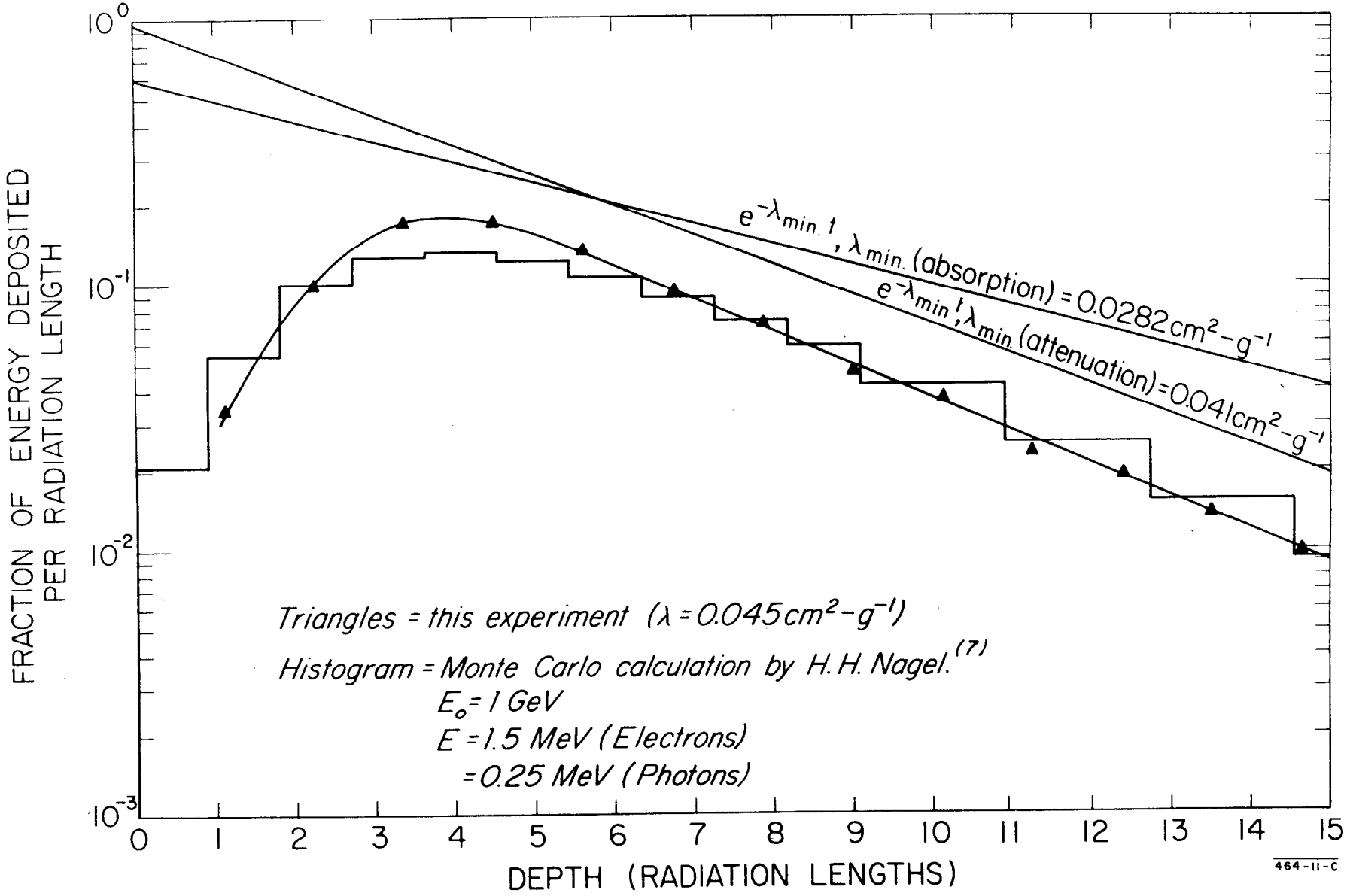
FRACTION OF ENERGY DEPOSITED PER RADIATION LENGTH
10^0
10^{-1}
10^{-2}
10^{-3}
$e^{-\lambda_{min.}t}, \lambda_{min.}$ (absorption) = 0.0282 cm^2-g^{-1}
$e^{-\lambda_{min}t}, \lambda_{min.}$ (attenuation) = 0.041 cm^2-g^{-1}
Triangles = this experiment (λ = 0.045 cm^2-g^{-1})
Histogram = Monte Carlo calculation by H. H. Nagel.[7]
E_o = 1 GeV
E = 1.5 MeV (Electrons)
= 0.25 MeV (Photons)
0 1 2 3 4 5 6 7 8 9 10 11 12 13 14 15
DEPTH (RADIATION LENGTHS)
464-11-C

Fig. 11

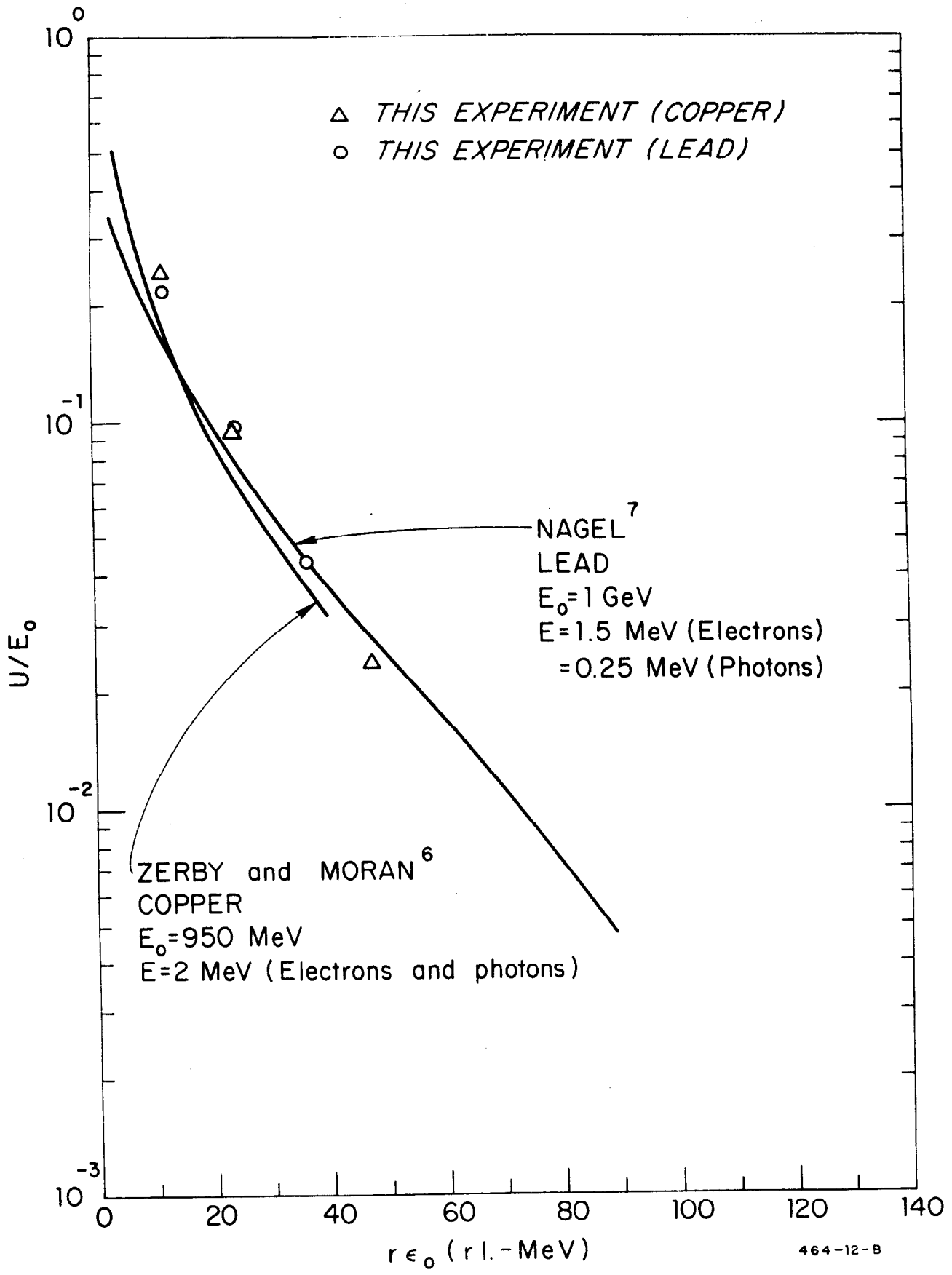
△ THIS EXPERIMENT (COPPER)
○ THIS EXPERIMENT (LEAD)
NAGEL[7]
LEAD
E_0=1 GeV
E=1.5 MeV (Electrons)
=0.25 MeV (Photons)
ZERBY and MORAN[6]
COPPER
E_0=950 MeV
E=2 MeV (Electrons and photons)
U/E_0
10^0
10^{-1}
10^{-2}
10^{-3}
0
20
40
60
80
100
120
140
$r\epsilon_0$ (r.l.-MeV)
464-12-B

Fig. 12

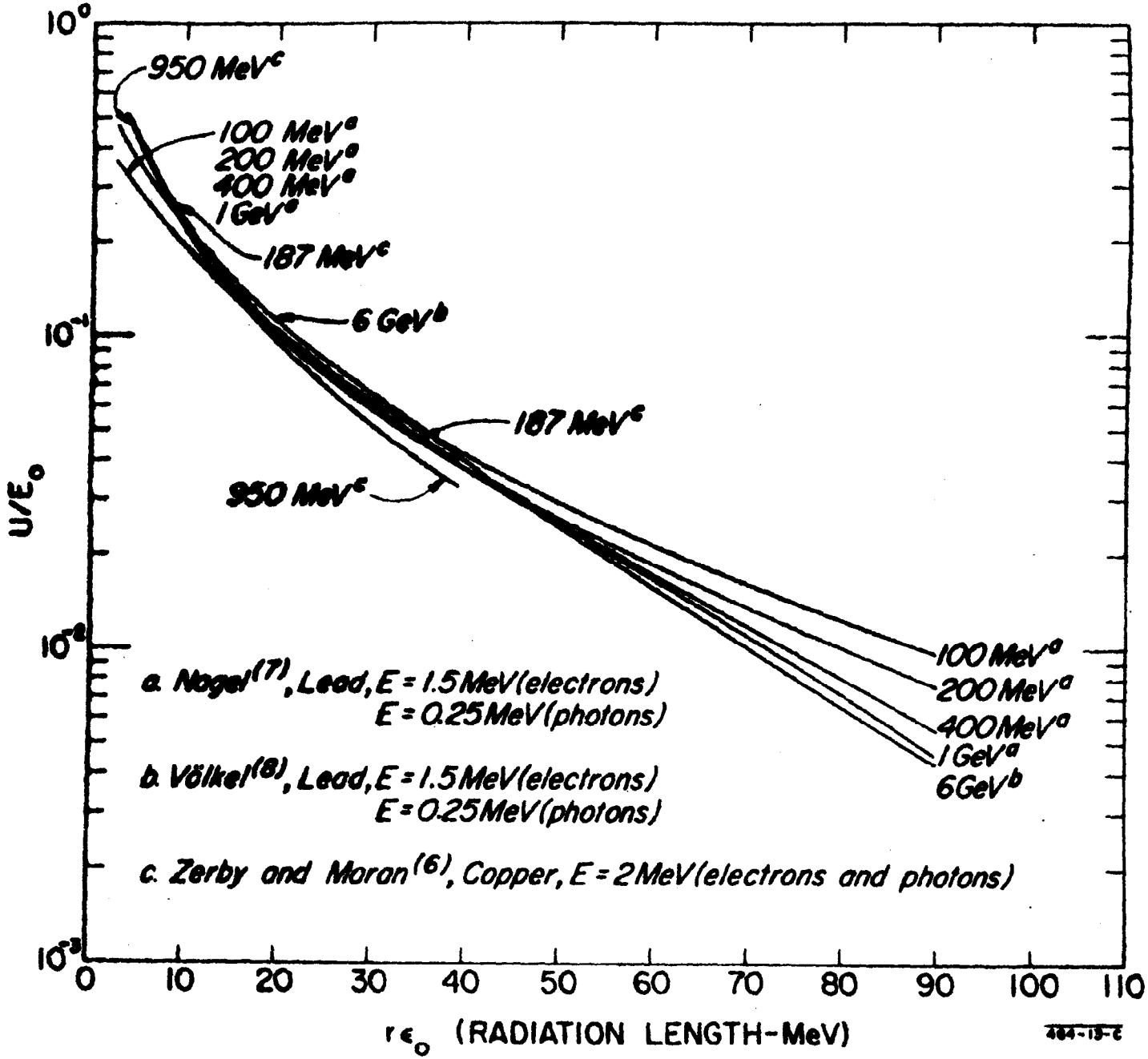
10°
10⁻¹
10⁻²
10⁻³
U/E₀
950 MeV^c
100 MeV^a
200 MeV^a
400 MeV^a
1 GeV^a
187 MeV^c
6 GeV^b
187 MeV^c
950 MeV^c
100 MeV^a
200 MeV^a
400 MeV^a
1 GeV^a
6 GeV^b
a. Nagel[7], Lead, E = 1.5 MeV (electrons)
E = 0.25 MeV (photons)
b. Völkel[8], Lead, E = 1.5 MeV (electrons)
E = 0.25 MeV (photons)
c. Zerby and Moran[6], Copper, E = 2 MeV (electrons and photons)
0
10
20
30
40
50
60
70
80
90
100
110
rε₀ (RADIATION LENGTH-MeV)
484-15-2

Fig. 13

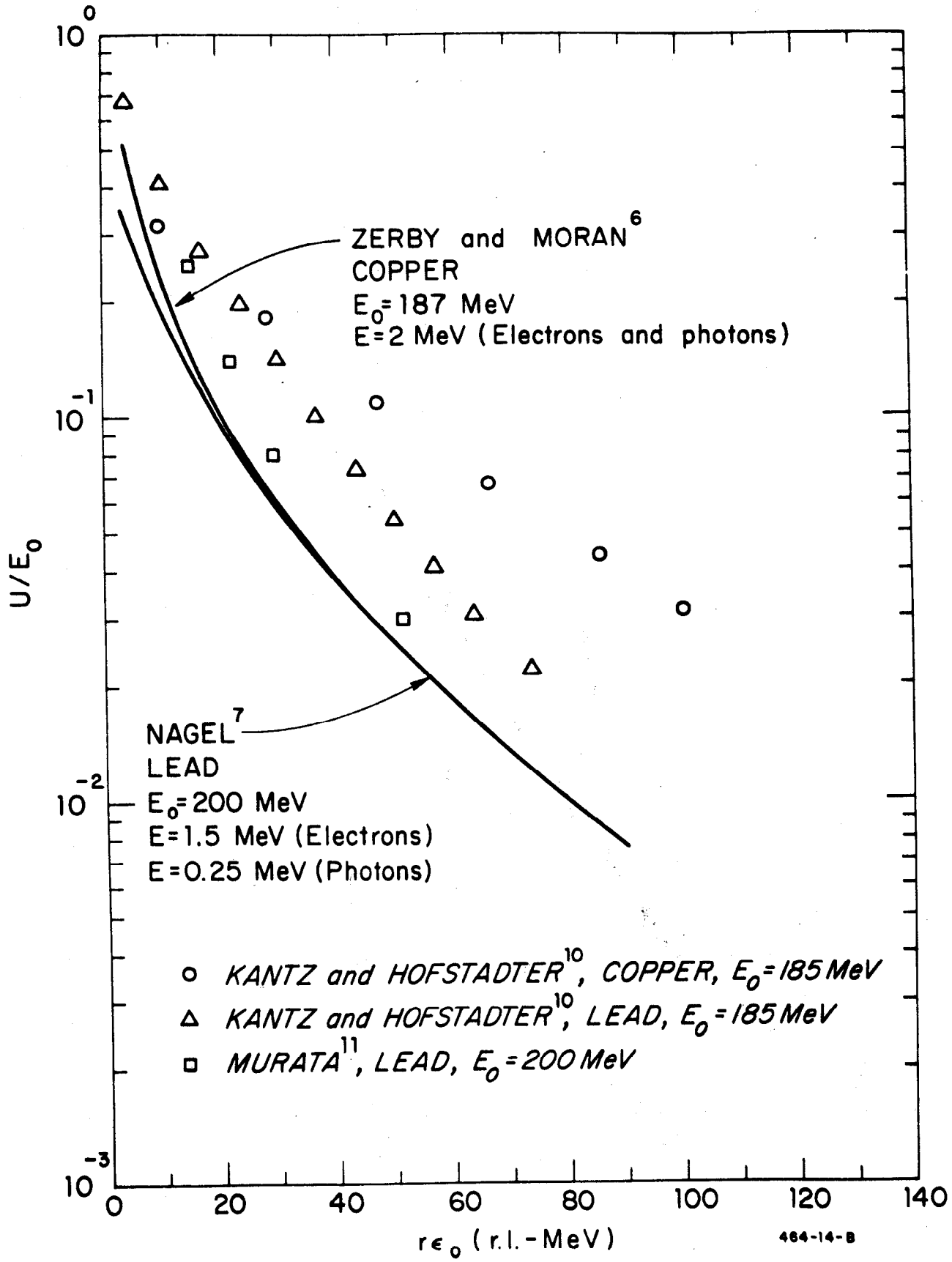
10^0
10^{-1}
10^{-2}
10^{-3}
U/E_0
ZERBY and MORAN[6]
COPPER
E_0=187 MeV
E=2 MeV (Electrons and photons)
NAGEL[7]
LEAD
E_0=200 MeV
E=1.5 MeV (Electrons)
E=0.25 MeV (Photons)
KANTZ and HOFSTADTER[10], COPPER, E_0=185 MeV
KANTZ and HOFSTADTER[10], LEAD, E_0=185 MeV
MURATA[11], LEAD, E_0=200 MeV
0
20
40
60
80
100
120
140
$r\epsilon_0$ (r.l.-MeV)
464-14-B

Fig. 14

TABLE I-A LEAD

String No. 1

Depth = 0.25 inch

Radial Increment (Units of 0.185 cm)	Normalized Energy Deposition (Roentgens)
0 - 6	0.36
6 - 12	2.23
12 - 18	320.0
18 - 20	23.5
20 - 24	3.02
24 - 30	0.52
30 - 42	0.12

TABLE I-B LEAD

String No. 2

Depth = 0.50 inch

Radial Increment (Units of 0.185 cm)	Normalized Energy Deposition (Roentgens)
0 - 6	0.23
6 - 12	0.57
12 - 15	1.55
15 - 18	5.54
18 - 20	22.4
20 - 21	65.7
21 - 22	210.6
22 - 23	1170.0
23 - 24	3000.0
24 - 25	790.0
25 - 26	147.0
26 - 28	33.8
28 - 30	9.76
30 - 33	2.74
33 - 39	0.70

TABLE I-C LEAD

String No. 3

Depth = 0.75 inch

Radial Increment (Units of 0.185 cm)	Normalized Energy Deposition (Roentgens)
0 - 6	0.38
6 - 9	0.77
9 - 12	1.85
12 - 14	3.96
14 - 16	10.84
16 - 18	35.7
18 - 19	111.7
19 - 20	428.0
20 - 21	2525.0
21 - 22	4600.0
22 - 23	1290.0
23 - 24	227.0
24 - 26	51.2
26 - 28	12.7
28 - 30	4.98
30 - 33	2.14
33 - 39	---
39 - 45	0.22

TABLE I-D LEAD

String No. 4

Depth = 1.00 inch

Radial Increment (Units of 0.185 cm)	Normalized Energy Deposition (Roentgens)
0 - 6	0.20
6 - 12	0.78
12 - 15	1.76
15 - 18	4.84
18 - 21	19.52
21 - 24	236.0
24 - 25	2470.0
25 - 26	3070.0
26 - 27	760.0
27 - 30	106.5
30 - 33	14.07
33 - 36	4.82
36 - 39	1.72
39 - 45	0.59

TABLE I-E LEAD

String No. 5

Depth = 1.25 inches

Radial Increment (Units of 0.185 cm)	Normalized Energy Deposition (Roentgens)
0 - 6	0.55
6 - 9	1.12
9 - 12	2.15
12 - 15	5.54
15 - 17	14.77
17 - 18	32.0
18 - 19	67.9
19 - 20	143.5
20 - 21	463.0
21 - 22	1340.0
22 - 23	1580.0
23 - 24	550.0
24 - 25	181.9
25 - 27	81.9
27 - 29	23.9
29 - 32	6.14
32 - 35	2.29
35 - 38	2.37

TABLE I-F LEAD

String No. 6

Depth = 1.50 inches

Radial Increment (Units of 0.185 cm)	Normalized Energy Deposition (Roentgens)
0 - 6	0.40
6 - 12	1.55
12 - 15	4.35
15 - 18	14.07
18 - 21	73.7
21 - 22	298.0
22 - 23	750.0
23 - 24	710.0
24 - 25	285.0
25 - 27	91.4
27 - 30	22.6
30 - 33	5.57
33 - 36	2.14
36 - 42	0.84

TABLE I-G LEAD

String No. 7

Depth = 1.75 inches

Radial Increment (Units of 0.185 cm)	Normalized Energy Deposition (Roentgens)
0 - 6	0.53
6 - 9	1.07
9 - 12	1.94
12 - 15	4.24
15 - 18	10.8
18 - 20	32.8
20 - 21	71.5
21 - 22	132.7
22 - 23	300.0
23 - 24	465.0
24 - 25	237.0
25 - 26	106.9
26 - 28	43.6
28 - 30	15.9
30 - 33	5.80

TABLE I-H LEAD

String No. 8

Depth = 2.00 inches

Radial Increment (Units of 0.185 cm)	Normalized Energy Deposition (Roentgens)
0 - 6	0.46
6 - 12	1.31
12 - 15	3.48
15 - 18	8.49
18 - 20	24.1
20 - 21	39.4
21 - 22	76.1
22 - 23	143.0
23 - 24	196.0
24 - 25	128.0
25 - 26	66.4
26 - 28	26.7
28 - 30	11.54
30 - 33	4.99

TABLE I-I LEAD

String No. 9

Depth = 2.25 inches

Radial Increment (Units of 0.185 cm)	Normalized Energy Deposition (Roentgens)
0 - 6	0.43
6 - 9	0.89
9 - 12	1.71
12 - 15	3.93
15 - 18	10.55
18 - 20	30.0
20 - 21	53.2
21 - 22	96.5
22 - 23	112.9
23 - 24	61.6
24 - 25	34.0
25 - 27	18.8
27 - 30	8.04
30 - 33	3.30
33 - 36	1.58
36 - 42	0.66
42 - 48	0.25

TABLE I-J LEAD

String No. 10

Depth = 2.50 inches

Radial Increment (Units of 0.185 cm)	Normalized Energy Deposition (Roentgens)
0 - 6	0.26
6 - 12	0.69
12 - 15	1.49
15 - 18	2.88
18 - 20	5.65
20 - 22	11.14
22 - 23	18.40
23 - 24	29.7
24 - 25	50.2
25 - 26	60.6
26 - 27	37.5
27 - 28	24.2
28 - 30	12.64
30 - 32	5.89
32 - 34	3.18
34 - 37	1.95
37 - 40	0.91
40 - 46	0.42

TABLE I-K LEAD

String No. 11

Depth = 2.75 inches

Radial Increment (Units of 0.185 cm)	Normalized Energy Deposition (Roentgens)
0 - 12	0.09
12 - 18	0.30
18 - 24	0.69
24 - 27	1.60
27 - 30	2.77
30 - 32	5.44
32 - 34	8.97
34 - 35	17.0
35 - 36	23.2
36 - 37	32.3
37 - 38	29.5
38 - 39	15.9
39 - 41	10.37
41 - 43	5.15
43 - 45	2.83
45 - 48	1.57
48 - 51	0.93
51 - 57	0.44
57 - 63	0.16

TABLE I-L LEAD

String No. 12

Depth = 3.00 inches

Radial Increment (Units of 0.185 cm)	Normalized Energy Deposition (Roentgens)
0 - 6	0.20
6 - 12	0.52
12 - 15	1.02
15 - 18	1.72
18 - 21	3.62
21 - 24	9.11
24 - 26	20.8
26 - 27	12.8
27 - 29	8.4
29 - 32	3.99
32 - 35	1.80
35 - 38	1.07
38 - 41	0.57
41 - 47	0.25

TABLE I-M LEAD

String No. 13

Depth = 3.25 inches

Radial Increment (Units of 0.185 cm)	Normalized Energy Deposition (Roentgens)
0 - 6	0.10
6 - 12	0.24
12 - 18	0.54
18 - 21	1.14
21 - 24	2.14
24 - 26	4.17
26 - 28	7.80
28 - 30	10.6
30 - 32	6.08
32 - 34	2.88
34 - 37	1.67
37 - 40	0.98
40 - 46	0.46
46 - 52	0.19

TABLE I-N LEAD

String No. 14

Depth = 3.50 inches

Radial Increment (Units of 0.185 cm)	Normalized Energy Deposition (Roentgens)
0 - 6	0.18
6 - 12	0.42
12 - 15	0.73
15 - 18	1.35
18 - 20	2.16
20 - 22	3.92
22 - 24	5.86
24 - 26	4.39
26 - 28	2.60
28 - 31	1.50
31 - 34	0.83
34 - 40	0.40
40 - 46	0.16

TABLE II-A COPPER

String No. 1

Depth = 0.25 inch

Radial Increment (Units of 0.185 cm)	Normalized Energy Deposition (Roentgens)
0 - 3	0.46
3 - 5	2.52
5 - 6	8.54
6 - 7	35.1
7 - 8	397.6
8 - 9	662.3
9 - 10	46.42
10 - 11	10.94
11 - 13	6.38
13 - 15	0.53

TABLE II-B COPPER

String No. 2

Depth = 0.50 inch

Radial Increment (Units of 0.185 cm)	Normalized Energy Deposition (Roentgens)
0 - 18	0.102
18 - 24	1.02
24 - 27	23.0
27 - 28	241.0
28 - 29	1900.0
29 - 30	354.0
30 - 31	53.9
31 - 33	10.7
33 - 36	1.41
36 - 48	0.19

TABLE II-C COPPER

String No. 3

Depth = 1.00 inch

Radial Increment (Units of 0.185 cm)	Normalized Energy Deposition (Roentgens)
0 - 12	0.35
12 - 18	8.98
18 - 20	157.0
20 - 21	1460.0
21 - 22	3400.0
22 - 23	626.0
23 - 24	137.0
24 - 27	23.7
27 - 30	---
30 - 33	0.84
33 - 45	0.23

TABLE II-D COPPER

String No. 4

Depth = 1.50 inches

Radial Increment (Units of 0.185 cm)	Normalized Energy Deposition (Roentgens)
0 - 12	0.21
12 - 18	0.81
18 - 24	12.7
24 - 26	173.0
26 - 27	1000.0
27 - 28	3550.0
28 - 29	1710.0
29 - 30	379.0
30 - 32	83.42
32 - 36	10.0
36 - 42	1.08
42 - 48	0.25

TABLE II-E COPPER

String No. 5

Depth = 2.00 inches

Radial Increment (Units of 0.185 cm)	Normalized Energy Deposition (Roentgens)
0 - 12	0.41
12 - 18	3.09
18 - 24	181.0
24 - 25	2400.0
25 - 26	2360.0
26 - 27	755.0
27 - 28	219.0
28 - 29	85.3
29 - 31	28.2
31 - 33	8.82
33 - 39	1.96
39 - 48	0.38

TABLE II-F COPPER

String No. 6

Depth = 2.50 inches

Radial Increment (Units of 0.185 cm)	Normalized Energy Deposition (Roentgens)
0 - 12	0.13
12 - 24	0.83
24 - 30	8.2
30 - 32	42.2
32 - 34	188.0
34 - 35	710.0
35 - 36	1780.0
36 - 37	1720.0
37 - 38	589.0
38 - 40	165.0
40 - 42	36.3
42 - 48	6.74
48 - 54	0.94
54 - 66	0.23

TABLE II-G COPPER

String No. 7

Depth = 3.00 inches

Radial Increment (Units of 0.185 cm)	Normalized Energy Deposition (Roentgens)
0 - 6	0.75
6 - 12	3.70
12 - 15	18.8
15 - 18	133.0
18 - 19	650.0
19 - 20	1300.0
20 - 21	900.0
21 - 22	359.0
22 - 24	112.0
24 - 27	24.6
27 - 30	5.55
30 - 33	1.98
33 - 36	0.98

TABLE II-H COPPER

String No. 9

Depth = 4.00 inches

Radial Increment (Units of 0.185 cm)	Normalized Energy Deposition (Roentgens)
0 - 6	0.46
6 - 12	1.38
12 - 18	6.33
18 - 21	29.6
21 - 24	172.6
24 - 25	441.0
25 - 26	288.0
26 - 28	109.0
28 - 30	34.0
30 - 33	12.7
33 - 36	4.23
36 - 42	1.53
42 - 48	0.52

TABLE II-I COPPER

String No. 11

Depth = 5.00 inches

Radial Increment (Units of 0.185 cm)	Normalized Energy Deposition (Roentgens)
0 - 6	0.96
6 - 12	4.70
12 - 14	14.5
14 - 16	36.4
16 - 17	76.1
17 - 18	136.0
18 - 19	140.0
19 - 20	80.2
20 - 22	39.2
22 - 24	15.5
24 - 26	7.14
26 - 30	3.16
30 - 36	1.06
36 - 42	0.37

TABLE II-J COPPER

String No. 13

Depth = 6.00 inches

Radial Increment (Units of 0.185 cm)	Normalized Energy Deposition (Roentgens)
0 - 6	0.34
6 - 12	0.80
12 - 18	2.27
18 - 20	6.01
20 - 22	10.6
22 - 23	20.3
23 - 24	30.7
24 - 25	57.1
25 - 26	77.6
26 - 27	45.1
27 - 28	24.4
28 - 30	13.0
30 - 32	6.4
32 - 34	2.94
34 - 36	1.83
36 - 42	0.92
42 - 48	0.30

TABLE II-K COPPER

String No. 15

Depth = 8.00 inches

Radial Increment (Units of 0.185 cm)	Normalized Energy Deposition (Roentgens)
0 - 12	0.30
12 - 18	1.23
18 - 21	4.33
21 - 24	17.0
24 - 27	6.05
27 - 30	2.00
30 - 36	0.75
36 - 42	0.30

TABLE III

VALUES OF RADIATION LENGTHS AND CRITICAL ENERGIES FOR VARIOUS MATERIALS

Material	Radiation Length $X_o(g\text{-}cm^{-2})$	Critical Energy ϵ_o(MeV) (with density effect)
Lead	6.4	7.4
Copper	13.0	18.8
Li^7F	39.8	65.3
Air	37.1	81[a]

[a] The correction for the density effect is negligibly small for gases and is not accounted for in this value.